Pergamon

Geochimica et Cosmochimica Acta, Vol. 66, No. 18, pp. 3293–3301, 2002

0016-7037/02 $22.00 + .00

PII S0016-7037(02)00924-9

Melt composition control of Zr/Hf fractionation in magmatic processes

ROBERT L. LINNEN[1,2,*] and HANS KEPPLER[2,3]

[1]Department of Earth Sciences, University of Waterloo, Waterloo, Ontario, Canada, N2L 3G1
[2]Bayerisches Geoinstitut, Universität Bayreuth, 95440 Bayreuth, Germany
[3]Mineralogisches Institut, Universität Tübingen, Wilhemstrasse 56, 72074 Tübingen, Germany

(*Received August* 15, 2001; *accepted in revised form April* 22, 2002)

Abstract—Zircon ($ZrSiO_4$) and hafnon ($HfSiO_4$) solubilities in water-saturated granitic melts have been determined as a function of melt composition at 800° and 1035°C at 200 MPa. The solubilities of zircon and hafnon in metaluminous or peraluminous melts are orders of magnitude lower than in strongly peralkaline melt. Moreover, the molar ratio of zircon and hafnon solubility is a function of melt composition. Although the solubilities are nearly identical in peralkaline melts, zircon on a molar basis is up to five times more soluble than hafnon in peraluminous melts. Accordingly, calculated partition coefficients of Zr and Hf between zircon and melt are nearly equal for the peralkaline melts, whereas for metaluminous and peraluminous melts D_{Hf}/D_{Zr} for zircon is 0.5 to 0.2. Consequently, zircon fractionation will strongly decrease Zr/Hf in some granites, whereas it has little effect on the Zr/Hf ratio in alkaline melts or similar depolymerized melt compositions.

The ratio of the molar solubilities of zircon and hafnon for a given melt composition, temperature, and pressure is proportional to the Hf/Zr activity coefficient ratio in the melt. The data imply that this ratio is nearly constant and probably close to unity for a wide range of peralkaline and similar depolymerized melts. However, it changes by a factor of two to five over a relatively small interval of melt compositions when a nearly fully polymerized melt structure is approached. For most ferromagnesian minerals in equilibrium with a depolymerized melt, $D_{Hf} > D_{Zr}$. Typical values of D_{Hf}/D_{Zr} range from 1.5 to 2.5 for clinopyroxene, amphibole, and titanite. Because of the change in the Hf/Zr activity ratio in the melt, the relative fractionation of Zr and Hf by these minerals will disappear or even be reversed when the melt composition approaches that of a metaluminous or peraluminous granite. It is thus not surprising that fractional crystallization of such granitic magmas leads to a decrease in Zr/Hf, whereas fractional crystallization of depolymerized melts tends to increase Zr/Hf. There is no need to invoke fluid metasomatism to explain these effects. Results demonstrate that for ions with identical charge and nearly identical radius, crystal chemistry does not alone determine relative compatibilities. Rather, the effect of changing activity coefficients in the melt may be comparable to or even larger than elastic strain effects in the crystal lattice.

1. INTRODUCTION

Zirconium and hafnium are quadrivalent at virtually all redox conditions in the Earth's mantle and crust and have similar radii. For example, the effective ionic radius in eightfold coordination is 0.84 Å for Zr and 0.83 Å for Hf (Shannon, 1976). In igneous systems, these elements are typically incompatible up to the point of saturation in a Zr-Hf phase, and because of their similar ionic radii, it might be expected that the Zr/Hf ratio of a magma series remains constant. However, it has been noted by several authors that Zr/Hf ratios can be variable (e.g., Jochum et al., 1986; Dupuy et al., 1992). It has been proposed that higher-than-chondritic Zr/Hf ratios in ocean island basalts can largely be explained by clinopyroxene fractionation (David et al., 2000). However, the same authors indicated that lower-than-chondritic Zr/Hf ratios in granitic rocks are still problematic, and they invoked metasomatism by fluorine-rich aqueous fluids as an explanation. Fluid metasomatism has been proposed elsewhere to account for nonchondritic Zr/Hf values in granitic rocks (Bau, 1996), but other authors maintain that this ratio can be explained by crystal fractionation (Pan, 1997). These interpretations were made without the benefit of knowing the relative solubilities of zircon ($ZrSiO_4$) and hafnon ($HfSiO_4$) in different granitic melts, critical experimental data that are lacking.

Zircon–hafnon solubility and the evolution of Zr/Hf in granitic melts are analogous to columbite–tantalite solubility and the evolution of Nb/Ta in granitic melts. The molar solubilities of manganocolumbite and manganotantalite are nearly equal in peralkaline granitic melts at a constant temperature and pressure, but in subaluminous to peraluminous granitic melts, manganotantalite is roughly three times more soluble than manganocolumbite (Linnen and Keppler, 1997). This is interpreted to reflect a lower melt activity coefficient for Ta relative to Nb and is used to show how the Nb/Ta ratio of evolved peraluminous granitic melts decreases as crystal fractionation progresses (Linnen and Keppler, 1997). In the work reported here, we have measured zircon and hafnon solubilities in water-saturated peralkaline to peraluminous granitic melts. From these data, we can calculate the partition coefficients of Zr and Hf between zircon and melt. The diffusivity of Hf in zircon is extremely slow (e.g., at 800°C, log D_{Hf} in zircon is estimated to be -36.3 $m^2\ s^{-1}$; Cherniak et al., 1997), and thus, experiments attempting to determine Hf partitioning between zircon and melt directly that use doped or natural Hf-rich zircon will be unsuccessful because diffusion within the crystal is needed to attain equilibrium. The method employed in this study only requires

* Author to whom correspondence should be addressed (rlinnen@uwaterloo.ca).

Table 1. Zircon solubility experiments.

Experiment	P (bar)	T (°C)	Days	ASI	ZrO_2 (wt%)	2σ (wt%)	Zr (mol/kg)
Zr800-0.6[a]	2000	800	42	0.64	2.91	0.14	0.237
Zr800-0.8[a]	2000	800	42	0.82	1.00	0.20	0.081
Zr800-0.9[a]	2000	800	42	0.94	0.33	0.04	0.027
Zr800-1.0[a]	2000	800	42	1.02	0.05	0.02	0.004
Zr1035-0.6[b]	2000	1035	13	0.64	3.79	0.12	0.307
Zr1035-0.8[b]	2000	1035	14	0.82	1.46	0.08	0.118
Zr1035-0.9[b]	2000	1035	14	0.94	0.68	0.18	0.056
Zr1035-0[b]	2000	1035	13	1.02	0.27	0.08	0.022
Zr1035-11[b]	2000	1035	14	1.13	0.11	0.02	0.009
Zr1035-12[b]	2000	1035	14	1.22	0.11	0.04	0.009

[a] Experiment conducted in Nimonic 105 autoclave.
[b] Experiment conduction in TZM autoclave.

Zr and Hf diffusion in hydrous silicate melts, which are many orders of magnitude faster than diffusion in zircon.

In addition to solubilities and zircon partition coefficients, these experiments also yield information on the changes of Zr/Hf melt activity coefficient ratios as a function of melt composition, which will affect mineral-melt partition coefficients in general. It will be shown that like Nb/Ta, the decrease in Zr/Hf ratio observed in many granitic suites can be explained by crystal fractionation.

2. EXPERIMENTAL

2.1. Starting Materials

Natural zircon from Miask, Ural (Keppler, 1993), was crushed and examined for impurities under a binocular microscope, and a size fraction of ~10 to 500 μm was used in zircon solubility experiments. Backscatter images of zircon grains indicate that the starting material is homogeneous, and Hf, Th, and U were not detected by energy dispersive analyses. This indicates that the zircon is near end member. Hafnon was synthesized in a piston cylinder apparatus in a Pt-Rh capsule. A stoichiometric $HfO_2 + SiO_2$ mixture plus water or a 5 wt% HF solution was sealed in the capsule and placed at 1400°C and 1.5 GPa for 24 h. Synthetic hafnon crystals are 1 to 10 μm, and hafnon was the only phase identifiable from X-ray powder diffraction patterns after the syntheses. However, some unreacted HfO_2 crystals were identified by electron microprobe analyses, discussed below.

Gels of six granitic compositions with molar Al/(Na + K) ratios (hereafter referred to as alumina saturation index, or ASI) of 0.64, 0.83, 0.94, 1.02, 1.13 and 1.22 were prepared from tetraethylorthosilicate, sodium and potassium carbonate, and aluminum nitrate, at constant SiO_2 (mol%) and Na/K ratio (for wt% oxide totals, see Linnen and Keppler, 1997). The subaluminous (ASI 1.02) composition ($Q_{37.5}$-$Or_{24.9}$-$Ab_{37.4}$-$C_{0.2}$) corresponds to the 200-MPa water-saturated haplogranite minimum. After synthesis, the gels were homogenized by grinding in an agate mortar.

2.2. Experimental Equipment and Method

The experimental conditions are summarized in Tables 1 and 2. Experiments were conducted either in cold-seal pressure vessels (made of Nimonic 105 Ni-Cr super alloy) with H_2O as the pressure medium or in rapid quench TZM (Titanium-Zirconrum-molybdenum alloy) bombs with Ar as the pressure medium, both at the Bayerisches Geoinstitut, Germany. Temperatures were measured with NiCr-Ni thermocouples in an external borehole of the autoclave (cold seal) or sheath (TZM) calibrated against an internal thermocouple. Temperature measurements are accurate to within ±15°C, including the effects of temperature gradients and intrinsic errors of the thermocouples. Pressures were measured with pressure transducers calibrated against a Heise gauge and are accurate to within ±5 MPa. Quenching in both types of autoclaves was close to isobaric. In the cold-seal vessels, quenching took ~5 min when compressed air was used, and in the rapid-quench TZM vessels, quenching occurred in 1 to 2 s. All capsules

Table 2. Hafnon solubility experiments.

Experiment	P (bar)	T (°C)	Days	ASI	HfO_2 (wt%)	2σ (wt%)	Hf (mol/kg)
Hf800-0.6	2000	800	21	0.64	6.84	0.18	0.325
Hf800-0.8	2000	800	21	0.82	2.44	0.86	0.116
Hf800-08r	2000	800	70	0.82	2.20	0.28	0.104
Hf800-0.9	2000	800	21	0.94	0.68	0.14	0.032
Hf800-09r	2000	800	70	0.94	1.22	0.38	0.058
Hf800-10	2000	800	42	1.02	0.46	0.12	0.022
Hf800-10r	2000	800	56	1.02	0.48	0.20	0.023
Hf800-10r2	2000	800	56	1.02	0.50	0.10	0.024
Hf800-11	2000	800	42	1.13	0.36	0.32	0.017
Hf800-12	2000	800	42	1.22	0.22	0.18	0.010
Hf1035-0.6	2000	1035	13	0.64	6.84	0.24	0.325
Hf1035-0.8	2000	1035	14	0.82	2.72	0.34	0.129
Hf1035-0.9	2000	1035	14	0.94	1.60	0.32	0.076
Hf1035-10	2000	1035	13	1.02	0.88	0.22	0.042
Hf1035-11	2000	1035	14	1.13	0.47	0.26	0.022
Hf1035-12	2000	1035	14	1.22	0.37	0.24	0.017

[a] Experiment conducted in Nimonic 105 autoclave.
[b] Experiment conducted in TZM autoclave.

were weighed before and after experiments to ensure that no leaks occurred during the experiments.

All of the zircon solubility experiments and most of the hafnon solubility experiments were dissolution experiments. Approximately 40 mg of granitic gel and 4 mg of zircon or hafnon crystals were loaded into gold capsules (length 10, inner diameter 2.0, outer diameter 2.2 mm) containing ~4 mg of distilled H_2O. The amount of water added ensured that all of the granitic melts were water-saturated at the pressure and temperature of the experiment. The capsule was welded shut, placed in a drying oven at 150°C, and then checked for weight loss. To confirm that the hafnon solubility results reflect equilibrium saturation, four additional solubility experiments at 800°C were conducted: dissolution–crystallization using a stoichiometric $HfO_2 + SiO_2$ mixture and using HfO_2 alone. In all three experiments, $HfSiO_4$ was the only Hf-bearing phase identified by X-ray diffraction of the run products, and the Hf saturation values are similar, discussed below.

2.3. Analytical Methods

The concentrations of ZrO_2 and HfO_2 in the experimental glasses were determined with a JEOL JXA 8600 electron microprobe (University of Western Ontario, London, Canada) with a 20-kV accelerating voltage, 60- to 100-nA beam current, and 10-μm beam diameter. The respective standards were Zr and synthetic $ZrSiO_4$ and $HfSiO_4$, and counting times ranged from 60 to 300 s. Na, K, Al, and Si (albite and orthoclase standards, 10-s counting times each) were analyzed at the same time for correction purposes. At least 15 analyses for each experiment were obtained. Analyses were obtained at a distance of ~10 μm from zircon crystals. A blank standard with a zircon crystal and Zr-free hydrous glass was also analyzed. From these analyses, it was determined that fluorescence from the zircon crystal was only a problem if the analytical point was <5 μm from a zircon crystal. Glasses with an ASI of 0.64 and containing approximately 1 wt% ZrO_2, 1 wt% HfO_2, 100 ppm ZrO_2, and 200 ppm HfO_2 were synthesized to verify the electron microprobe analyses. The glasses were independently analyzed by inductively coupled plasma mass spectrometry. The electron microprobe analyses with 2σ standard deviation compare favorably with the inductively coupled plasma analyses (in parentheses): 1.20 ± 0.06% ZrO_2 (1.06), 0.01 ± 0.008% ZrO_2 (0.010), 0.92 ± 0.04% HfO_2 (0.914) and 0.028 ± 0.027% HfO_2 (0.024). The good correspondence of the two methods indicates that the electron microprobe analyses are accurate.

Powder diffraction patterns (10 to 80°2θ) of all run products were measured at the Bayerisches Geoinstitut on a Stoe STADIP powder diffractometer with monochromatized Co Kα_1 radiation. Zircon or hafnon were the only phases identified, although microscopy and electron microprobe analyses indicate that each of the hafnon dissolution experiments contain a minor amounts of unreacted HfO_2.

3. RESULTS

The dissolution of zircon and hafnon in a silicate melt can be described by the equations

$$ZrSiO_4^{zircon} = ZrO_2^{melt} + SiO_2^{melt} \quad (1)$$

$$HfSiO_4^{hafnon} = HfO_2^{melt} + SiO_2^{melt} \quad (2)$$

with the equilibrium constants

$$K_{ZrSiO_4} = a_{ZrO_2}^{melt} \times a_{SiO_2}^{melt}/a_{ZrSiO_4}^{zircon} \quad (3)$$

$$K_{HfSiO_4} = a_{HfO_2}^{melt} \times a_{SiO_2}^{melt}/a_{HfSiO_4}^{zircon}, \quad (4)$$

where a denotes activities. If pure zircon and pure hafnon coexist with the melts, as in our experiments, the activities of solid $ZrSiO_4$ and $HfSiO_4$ are equal to 1, and therefore

$$K_{ZrSiO_4} = a_{ZrO_2}^{melt} \times a_{SiO_2}^{melt} = \gamma_{ZrO_2}^{melt} \times X_{ZrO_2}^{melt} \times \gamma_{SiO_2}^{melt} \times X_{SiO_2}^{melt} \quad (5)$$

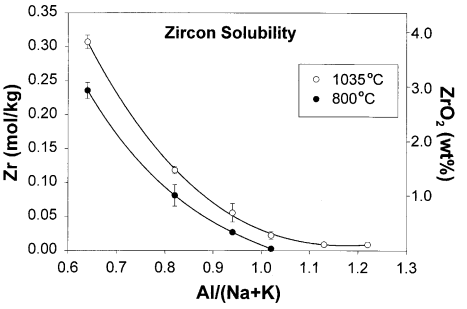

Fig. 1. Zircon solubility in granitic melts at 200 MPa and water-saturated conditions. Solid circles represent the compositions of glasses quenched from 800°C experiments and open circles from 1035°C experiments. Glass compositions are expressed as molar Al/(Na + K) ratios. Error bars represent 2σ standard deviation of the ZrO_2 content in glasses.

$$K_{HfSiO_4} = a_{HfO_2}^{melt} \times a_{SiO_2}^{melt} = \gamma_{HfO_2}^{melt} \times X_{HfO_2}^{melt} \times \gamma_{SiO_2}^{melt} \times X_{SiO_2}^{melt}, \quad (6)$$

where γ are activity coefficients and X are mole fractions. The mole fraction of SiO_2 for all the melt compositions considered here is constant. Analyses natural rocks and data from other experimental studies are normally reported in weight units of dissolved Zr or Hf. For an easier comparison, zircon and hafnon solubilities are therefore reported as mole fractions or ZrO_2 and HfO_2 (wt%), respectively, rather than as solubility products.

The results of the zircon solubility experiments are summarized in Table 1. Zircon solubility is governed primarily by melt composition, and to a lesser extent by temperature (Fig. 1). At 1035°C, 200 MPa and water-saturated conditions zircon solubilities decrease continuously from peralkaline (ASI 0.64; 3.8 wt% ZrO_2) through subaluminous (ASI 1.02; 0.27 wt% ZrO_2) to peraluminous (ASI 1.22; 0.11 wt% ZrO_2) melt compositions. Although experiments were not reversed, diffusion profiles for Zr can be calculated at 1035°C by means of the diffusion data of Harrison and Watson (1983) for obsidian with an ASI of 1.1 and 6 wt% H_2O. By use of this data, together with a distance of 10 μm, the typical distance from a zircon crystal that the analysis was acquired, it can be estimated that the relative amount that solubilities are underestimated is only 2 to 3%. This amount is much less than most of the 2σ errors given in Table 1. It should also be noted that Zr diffusion will be faster in less viscous alkaline melts, so that the relative error caused by diffusion problems in these melts will be even smaller. A few electron microprobe traverses were conducted, and it was concluded that Zr concentrations in glasses at a distance of 10 μm from zircon crystals are a reasonable estimate of Zr concentrations at the zircon–melt interface, and that coupled major element diffusion was not significant.

At 800°C, 200 MPa and water-saturated conditions, zircon solubilities range from nearly 3 wt% ZrO_2 for strongly peralkaline melts (ASI 0.64) to approximately 500 ppm ZrO_2 for the subaluminous composition (ASI 1.02). Zircon solubilities in the peraluminous melt compositions at 800°C and 200 MPa are <100 ppm ZrO_2. Even though the run times for these experiments were long, the diffusion data of Harrison and Watson

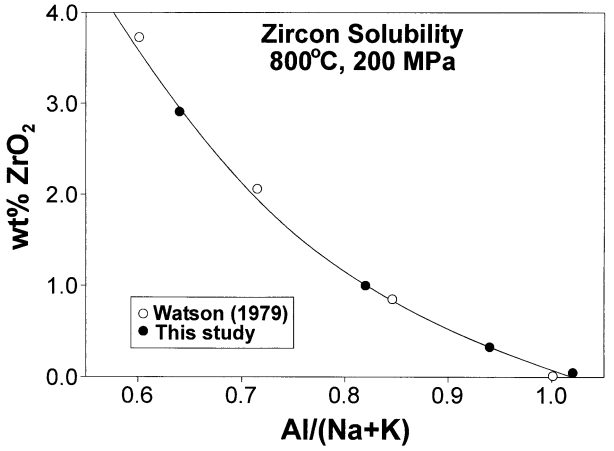

Fig. 2. Comparison of the results of zircon solubility in granitic melts at 800°C and 200 MPa from this study (solid circles) with those of Watson (1979) (open circles). Glass compositions are expressed as molar Al/(Na + K) ratios.

(1983) suggest that solubilities may have been underestimated by approximately 10 to 15%. This is a comparatively small error, and the consistency of our results with previous studies (Watson, 1979; Watson and Harrison, 1983; Keppler, 1993) suggests that the values in this study represent zircon solubilities (Figure 2).

The results of the hafnon solubility experiments are summarized in Table 2 and Fig. 3. For a given melt composition, temperature, and pressure, hafnon is always more soluble than zircon (either in terms of wt% or mol/kg). The solubility of hafnon is otherwise similar to that of zircon, increasing strongly with the alkali content of the melt, and to a lesser extent increasing with temperature. Repeat experiments, involving dissolution of and reaction of HfO_2 to form $HfSiO_4$ (the r experiments in Table 2) or of a stoichiometric mixture of HfO_2 and SiO_2 (the r2 experiment in Table 2) are within the 2σ standard deviation of the results from the hafnon dissolution experiments: 2.44 ± 0.86 vs. 2.20 ± 0.28 wt% HfO_2 for experiments Hf800 to 0.8 and Hf800 to 0.8r, respectively; and 0.46 ± 0.12, 0.48 ± 0.20 and 0.50 ± 0.10 wt% HfO_2 for experiments Hf800 to 10, Hf800 to 10r and Hf800 to 10r2, respectively. The consistency of the results indicates that equilibrium was attained. The only experiment set where there is a problem is Hf800 to 0.9 and Hf800 to 0.9r, where there is a larger spread 0.68 ± 0.14 vs. 1.22 ± 0.38 wt% HfO_2, respectively. However, the average of these two experiments does give a value consistent with the compositional trend on Figure 3.

4. DISCUSSION

4.1. Zr and Hf Speciation in Silicate Melts

Figure 4 shows the zircon and hafnon solubility data for the subaluminous to peralkaline melt compositions in terms of mol/kg Na+K-Al vs. the excess mol/kg of Zr or Hf. The latter is the number of moles of Zr or Hf in a given zircon- or hafnon-saturated melt composition, minus the number of moles of Zr or Hf for the zircon- or hafnon-saturated subaluminous composition at the same T and P, it quantifies the "peralkaline effect" on solubility. It has previously been shown that the dissolution of one mole of excess Zr requires two moles of excess Na_2O or K_2O (Watson, 1979). The explanation given for this observation is that four nonbridging oxygens, supplied

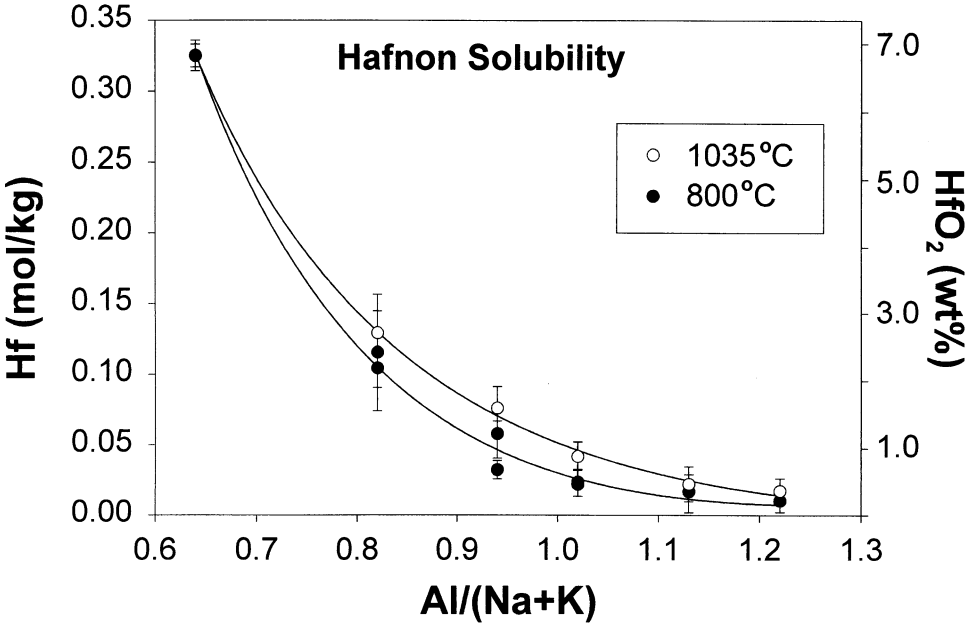

Fig. 3. Hafnon solubility in granitic melts at 200 MPa and water-saturated conditions. Solid circles represent the compositions of glasses quenched from 800°C experiments and open circles from 1035°C experiments. Glass compositions are expressed as molar Al/(Na + K) ratios. Error bars represent 2σ standard deviation of the Hf content in glasses.

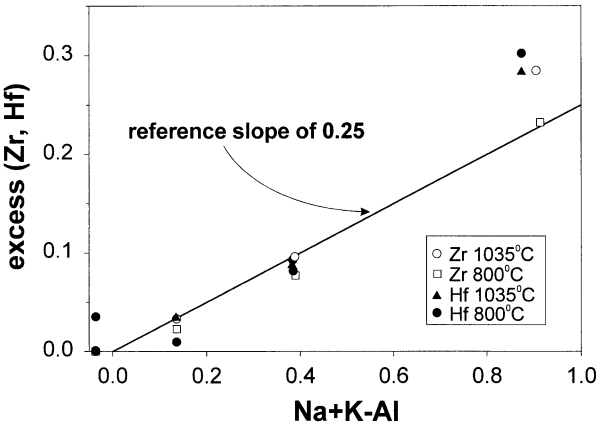

Fig. 4. Relationship between the excess moles of Zr or Hf vs. the excess moles of alkalis (Na+K-Al) from zircon and hafnon solubility experiments in water-saturated granitic melts at 800°C and 1035°C at 200 MPa. The former is the number of moles of Zr or Hf in an alkaline granitic glass minus the number of moles of Zr or Hf in the subaluminous (ASI = 1.0) glass quenched from experiments at the same temperature and pressure.

by four alkali cations, stabilize each Zr^{4+} cation (Hess, 1991). The Zr and Hf data for moderately peralkaline melts on Figure 4 support the idea that both these 4^+ cations dissolve by such a process because the slope is close to 0.25. However, the strongly peralkaline (ASI 0.64) experiments seem to contain anomalously high concentrations of Zr and Hf. This may be related to the fact the starting compositions of the glasses were chosen such that the mole fraction of SiO_2 was constant. The activity of SiO_2 in the strongly peralkaline melt is lower than that of moderately peralkaline melts at the same temperature and pressure, and because $ZrSiO_4$ and $HfSiO_4$ solubilities depend on the activity of SiO_2 in the melt, more ZrO_2 or HfO_2 can be dissolved in the melt with the lower SiO_2 activity. The apparent similarity of Zr and Hf speciation in peralkaline melts suggests that the activity coefficients of these two elements in the melt are nearly equal.

4.2. Zr and Hf Partitioning between Zircon and Melt

The unit cell volume of hafnon is only 1.24% smaller than that of zircon, and the hafnon structure otherwise is essentially identical to the zircon structure (Speer and Cooper, 1982). Therefore, the solid solution between zircon and hafnon is most likely close to an ideal mixture. With the assumption of ideal mixing in the crystal, the ratio D_{Hf}/D_{Zr} of the partition coefficients of Zr and Hf between a zircon–hafnon solid solution and the silicate melt is simply given by the ratio of zircon to hafnon solubility, as expressed by the molar fractions of Zr and Hf dissolved in the melt in equilibrium with pure hafnon and zircon. This can be seen in the following way: dividing Eqn. 3 by Eqn. 4 yields

$$\frac{K_{ZrSiO_4}}{K_{HfSiO_4}} = \frac{a^{melt}_{ZrO_2} \times a^{zircon_{ss}}_{HfSiO_4}}{a^{melt}_{HfO_2} \times a^{zircon_{ss}}_{ZrSiO_4}} \quad (7)$$

With the assumption of ideal mixing in the zircon–hafnon solid solution, that is,

$$\gamma_{ZrSiO_4} = \gamma_{HfSiO_4} = 1. \quad (8)$$

This can be rearranged to

$$\frac{K_{ZrSiO_4} \times \gamma^{melt}_{HfO_2}}{K_{HfSiO_4} \times \gamma^{melt}_{ZrO_2}} = \frac{X^{melt}_{ZrO_2} \times X^{zircon_{ss}}_{HfSiO_4}}{X^{melt}_{HfO_2} \times X^{zircon_{ss}}_{ZrSiO_4}} = \frac{D^{zircon\text{-}melt}_{Hf}}{D^{zircon\text{-}melt}_{Zr}} \quad (9)$$

where $D^{zircon\text{-}melt}_{Hf}$ and $D^{zircon\text{-}melt}_{Zr}$ are the zircon-melt partition coefficients of Hf and Zr, respectively. However, dividing Eqn. 5 by Eqn. 6 yields

$$\frac{K_{ZrSiO_4} \times \gamma^{melt}_{HfO_2}}{K_{KfSiO_4} \times \gamma^{melt}_{ZrO_2}} = \frac{X^{melt}_{ZrO_2}}{X^{melt}_{HfO_2}} \quad (10)$$

where $X^{melt}_{ZrO_2}$ and $X^{melt}_{HfO_2}$ are the molar fractions of Zr and Hf in a melt in equilibrium with pure zircon and hafnon, respectively. Combining Eqns. 9 and 10 yields

$$\frac{X^{melt}_{ZrO_2}}{X^{melt}_{HfO_2}} = \frac{D_{Hf}}{D_{Zr}} \quad (11)$$

The ratio of the molar fractions of Zr and Hf dissolved in a melt in equilibrium with pure zircon or hafnon, respectively, is plotted in Figure 5. According to Eqn. 11, this yields directly the ratio D_{Hf}/D_{Zr} for a zircon solid solution in equilibrium with a silicate melt.

From Figure 5, it is obvious that for depolymerized peralkaline melts D_{Hf}/D_{Zr} is close to unity over a wide range of melt compositions, particularly at high temperatures. However, when the melt approaches subaluminous or peraluminous compositions, D_{Hf}/D_{Zr} decreases to 0.5 to 0.2. This decrease occurs over a relatively narrow interval of compositions. Accordingly, crystallization of zircon does by no means always lead to a fractionation of Zr and Hf. In depolymerized melts, little or no fractionation will occur, whereas a selective depletion of zirconium relative to hafnium is to be expected in some subaluminous or peraluminous granitic suites. Absolute values of $D^{zircon\text{-}melt}_{Hf}$ as calculated from the solubility data range from 10 for strongly peralkaline compositions to 300 for the peraluminous composition studied.

4.3. Effect of Melt Composition on Zr/Hf Fractionation by Various Minerals

Zircon is certainly the most important phase for the fractionation of Zr and Hf. However, some ferromagnesian minerals and some accessory phases may also fractionate Zr from Hf. Table 3 is a compilation of relevant mineral/melt partition coefficients; some additional data are in Green (1994). Zr and Hf are mildly incompatible in clinopyroxene and amphibole and mildly incompatible to mildly compatible in garnet, which means that crystallization of these phases will only slightly affect Zr/Hf ratios. However, data from natural samples suggest that ilmenite and titanite may strongly concentrate Zr and Hf (Della Ventura et al., 1999, Bingen et al., 2001). With the notable exception of garnet, all minerals prefer Hf over Zr in equilibrium with depolymerized melts, such as basalts, basanites, and phonolites. By use of our data on zircon and hafnon solubility as a function of melt composition, we can now at least roughly predict how the relative fractionation of Zr and Hf between these minerals and silicate melts change as these melts

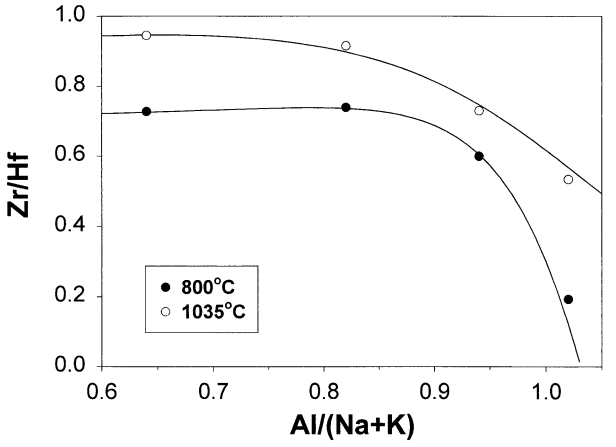

Fig. 5. The molar Zr/Hf ratio from zircon and hafnon solubility experiments in the same granitic composition conducted at 200 MPa. Solid circles represent the compositions of glasses quenched from 800°C experiments and open circles from 1035°C experiments. Glass compositions are expressed as molar Al/(Na + K) ratios.

approach subaluminous and peraluminous granitic compositions.

The ratio of the equilibrium constants, K_{ZrSiO_4}/K_{HfSiO_4}, is a function of temperature and pressure only. Consequently, Eqn. 10 implies that if the measured molar solubilities of zircon and hafnon for a fixed melt composition, temperature, and pressure are divided, the resulting number is proportional to the activity coefficient ratio, $\gamma^{melt}_{HfO_2}/\gamma^{melt}_{ZrO_2}$, in the melt. When elements are partitioned between melts and minerals, the chemical potentials of the element or oxide component in the two phases is equal. Consequently, if the activity coefficient ratio remains constant with variable melt composition, then a mineral-melt partition coefficient ratio, D_{Hf}/D_{Zr}, will also be constant (at fixed P, T), independent of melt composition. If on the other hand $\gamma^{melt}_{HfO_2}/\gamma^{melt}_{ZrO_2}$ changes with melt composition, then for any mineral, D_{Hf}/D_{Zr}, will also vary as a function of melt composition—that is, any change of the melt activity coefficient will cause a corresponding change in the mineral-melt partition coefficient.

The zircon/hafnon molar solubility ratios are shown in Figure 5. It is apparent that for alkaline, depolymerized compositions this ratio is constant, suggesting that mineral-melt partition coefficients will also be constant for a range of compositions. As the melt composition approaches that of subaluminous or peraluminous granites, however, the ratio of $\gamma^{melt}_{HfO_2}/\gamma^{melt}_{ZrO_2}$ decreases by a factor of 2 to 5. All other parameters remaining equal, this will decrease D_{Hf}/D_{Zr} by the same factor. According to the data in Table 3, this is sufficient to make the relative fractionation of Zr and Hf between melt and minerals such as amphibole, clinopyroxene, and titanite disappear or even to reverse it. We therefore conclude that the partitioning behavior of ions with similar ionic radius, such as Zr^{4+} and Hf^{4+}, is not solely controlled by elastic strain effects in the crystal lattice (for effects on the latter, see Brice, 1975; Blundy and Wood, 1994). Rather, the magnitude of the effect of changing activity coefficients in the melt is at least comparable to the strain effects in the crystal.

The changes in the activity coefficient ratio of Zr and Hf may be because in fully polymerized melts, there are no nonbridging oxygen atoms available to locally charge compensate the Zr^{4+} and Hf^{4+} ions. In this situation, probably some more covalent interactions between these ions and surrounding oxygen atoms become important. The different behavior of Zr and Hf may therefore be related to the significantly different electronegativities of these elements (1.4 for Zr, 1.3 for Hf; Greenwood and Earnshaw, 1984).

4.4. Zr/Hf Fractionation in Magmatic Systems

From the discussion above, the following can be concluded. (1) In alkaline or depolymerized melts, zircon solubility is high and even if zircon crystallizes, it does not significantly fractionate Zr from Hf. Clinopyroxene, amphibole and titanite will

Table 3. Some experimentally measured mineral/melt partition coefficients of zirconium and hafnium.

Mineral	Reference[a]	Melt composition	T (°C)	P (GPa)	D_{Zr}	D_{Hf}	D_{Hf}/D_{Zr}
Garnet	1	Basanite	1050	2.5	0.23	0.10	0.44
Garnet	2	Basanite, tholeite	1080–1200	2–7.5	0.12 to .061	0.07 to 0.41	0.58 to 1.33
Garnet	3,4	Ultramafic, basaltic	1530–1565	3	0.3 to 3.6	0.38 to 2.4	0.7 to 1.7
Clinopyroxene	2	Basanite, tholeite	1530–1565	2–7.5	0.04 to 0.18	0.07 to 0.31	1.7 to 2.45
Clinopyroxene	5	Alkali basalt	1380	3	0.12	0.26	2.2
Orthopyroxene	2	Basanite, tholeite	1080–1200	2–7.5	0.03	0.06	1.88
Pyroxene	4	Ultramafic	1540	3	0.04	0.05	1.3
Amphibole	1	Basanite	1000	1	0.24	0.37	1.5
Amphibole	6	Tonalite	850	1	0.42	0.66	1.6
Amphibole	7	Andesite	1000	1.5	0.23	0.45	2.0
Titanomagnetite	1	Basanite	1050	1.5	~0.8	~0.8	10
Titanite	8	Phonolite	—[b]	—[b]	~4	~10	2.5

[a] 1, Fujinawa and Green (1997); 2, Green et al. (2000); 3, van Westrenen et al. (1999); 4, van Westrenen et al. (2000); 5, Hart and Dunn (1993); 6, Klein et al. (1997); 7, Brenan et al. (1995); 8, Wörner et al. (1983).

[b] These data are from analyses of natural titanites and the coexisting glass phase, not from experimental samples.

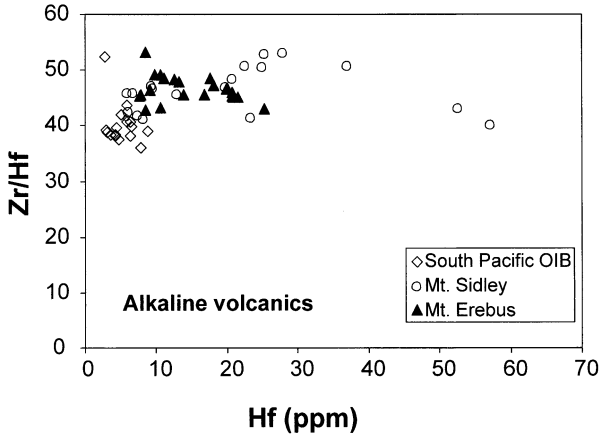

Fig. 6. Relationship between the Zr/Hf weight ratio and Hf in alkaline volcanic rocks from Mt. Erebus (Kyle et al., 1992), Mt. Sidley (Panter et al., 1997), and South Pacific ocean island basalts (Hauri and Hart, 1997).

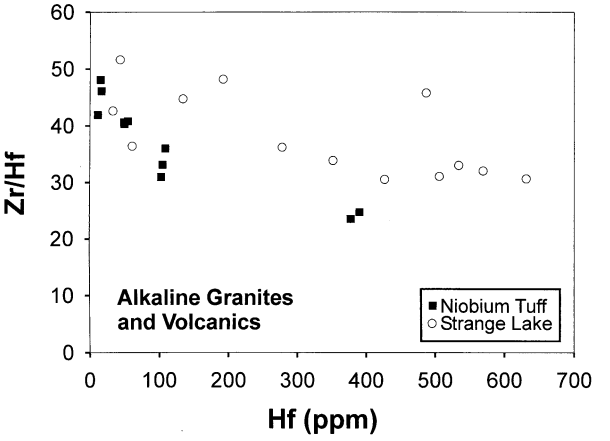

Fig. 7. Relationship between the Zr/Hf weight ratio and Hf in alkaline granites and volcanics from Niobium Tuff (Taylor et al., 1995) and Strange Lake (Boily and Williams-Jones, 1994).

preferentially incorporate Hf over Zr and the fractional crystallization of these minerals will therefore tend to slightly increase Zr/Hf in the residual melt. However, the effect will be small or negligible if only amphibole and clinopyroxene are present, as Zr and Hf are mildly incompatible in these minerals. Only garnet may preferentially incorporate Zr, but in the presence of clinopyroxene, the effects of these two minerals will tend to cancel out. Therefore, in alkaline or other depolymerized silicate melts, mineral fractionation should either leave Zr/Hf nearly unchanged or slightly increase this ratio. (2) In subaluminous or peraluminous granites the situation is fundamentally different. Zircon solubility is low and zircon now strongly fractionates Zr from Hf. Moreover, all other minerals considered above either do not fractionate Zr from Hf anymore or they fractionate it in the same direction as zircon. Accordingly, in subaluminous and peraluminous granites, a strong decrease of Zr/Hf is expected to occur with fractional crystallization.

These predictions are in perfect agreement with most field observations. A near constant Zr/Hf ratio is observed in many suites of alkaline volcanic rocks (Fig. 6)—for example, Mt. Erebus (Kyle et al., 1992), Mt. Sidley (Panter et al., 1997), and ocean island basalts from the South Pacific (Hauri and Hart, 1997). On this figure, increasing Hf concentrations are assumed to reflect increasing degrees of differentiation, an assumption that is supported by a strong positive correlation between Hf and K_2O in these suites. Even in highly fractionated alkaline granites and volcanics, where several hundred parts per million Hf was in the melt, the Zr/Hf ratio is typically not greatly different from the chondritic ratio—for example, Strange Lake (Boily and Williams-Jones, 1994) and the Brockman volcanics (Taylor et al., 1995) (Fig. 7).

The occurrence of hafnium-rich zircon in many highly evolved granitic pegmatites (e.g., Tanco; Cerny and Siilova, 1980) and granites (e.g., Suzhou; Wang et al., 1996) can be explained by crystal fractionation. The strong decrease in the Zr/Hf ratio observed in many highly fractionated peraluminous granites (Fig. 8), (e.g., Beauvoir; Raimbault et al., 1995) and Argemela (Charoy and Noronha, 1996), and rhyolites (e.g., Macusani; Pichavant et al., 1988) and Ongonite (Kortemeirer and Burt, 1988) can also be explained by crystal fractionation without the need to invoke metasomatism. Increasing Hf concentration is again assumed to reflect increasing degrees of differentiation. At Beauvoir, there is a positive correlation between Hf and Rb and a negative correlation between Hf and Ti, indicating that this assumption is probably reasonable, at least for this suite.

However, a decrease in Zr/Hf with increasing Hf is not observed universally in granitic suites. Figure 9 shows Zr/Hf vs. Hf data for three metaluminous and peraluminous granitic suites. In the case of the Erzgebirge granites of Germany, there is an apparent positive correlation between Zr/Hf and Hf. However, at Erzgebirge, there is also a positive correlation between Hf and TiO_2, and a negative correlation between Hf and Rb, implying that for this suite, Hf is compatible. In addition, the most evolved granites contain zircons with the lowest Zr/Hf ratios and the lowest Zr and Hf abundances. These

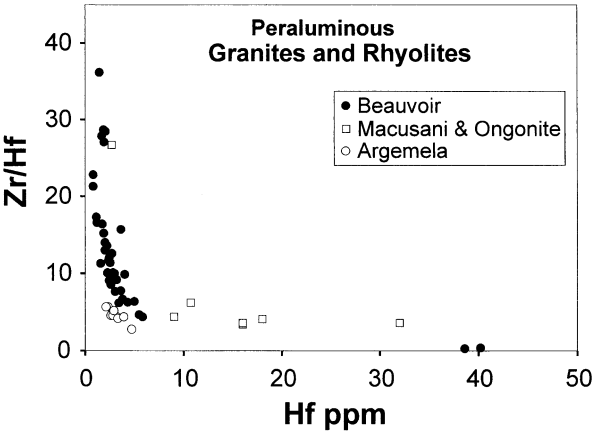

Fig. 8. Relationship between the Zr/Hf weight ratio and Hf in peraluminous granites Beauvoir (Raimbault et al., 1995), Argemela (Charoy and Noronha, 1996), and volcanics Macusani (Pichavant et al., 1988) and Ongonite (Kortemeirer and Burt, 1988).

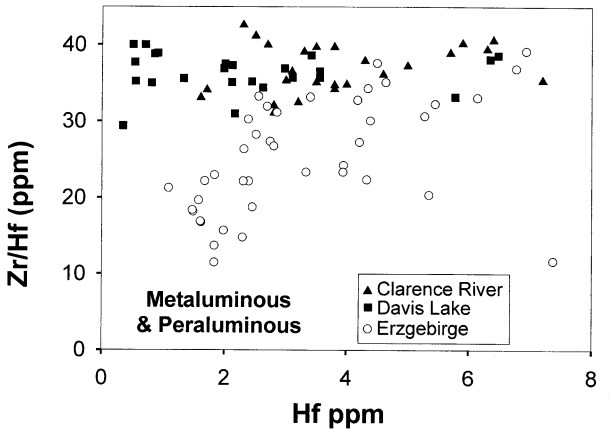

Fig. 9. Relationship between the Zr/Hf weight ratio and Hf in metaluminous and peraluminous granites from Clarence River (Bryant et al., 1997), Davis Lake (Dostal and Chatterjee, 1995), and Erzgebirge (Förster et al., 1999).

lower abundances are interpreted to be the result of lower solubilities at lower temperature (Förster et al., 1999). In the cases of the Clarence River (Bryant et al., 1997) and Davis Lake (Dostal and Chatterjee, 1995) suites, the Zr/Hf ratios are nearly constant. In both these cases, Hf decreases with TiO_2, suggesting that Hf is a compatible element. Potential explanations are that crystallization occurred over a narrow temperature range and that the ASI ratio of the melt was nearly constant. If crystallization were dominated by quartz and feldspar (which incorporate little Zr and Hf) and little zircon crystallizes, then the Zr/Hf ratio of the residual melt may decrease very little. Alternatively, if these suites contained restite zircon, the Zr/Hf ratio of these zircons may have buffered the Zr/Hf ratio of the melt.

It is intriguing that the strongly depleted Zr/Hf ratios in Fig. 8 are associated with fluorine-rich melts. The high F contents result in higher zircon–hafnon solubility (Keppler, 1993) and make it less likely that restite zircons survive (which could control whole-rock Zr/Hf). The increased zircon solubility (which could also result from higher temperature melts) provides optimal conditions for zircon crystal fractionation, which in turn results in the dramatic decrease of the whole-rock or zircon Zr/Hf ratio.

Acknowledgments—We thank H. Schulze for the preparation of polished sections and Yves Thibault for help with the electron microprobe analyses. We are also grateful for comments by Calvin Miller and two anonymous reviewers.

Associate editor: C. Romano

REFERENCES

Bau M. (1996) Controls on the fractionation of isovalent trace elements in magmatic and aqueous systems: Evidence from Y/Ho, Zr/Hf and lanthanide tetrad effect. *Contrib. Mineral. Petrol.* **123,** 323–333.

Bingen B., Austrheim H., and Whitehouse M. (2001) Ilmenite as a source for zirconium during high-grade metamorphism? Textural evidence from the caledonides of western Norway and implications for zircon geochronology. *J. Petrol.* **42,** 355–375.

Blundy J. D. and Wood B. J. (1994) Prediction of crystal-melt partition coefficients from elastic moduli. *Nature* **372,** 452–454.

Boily M. and Williams-Jones A. E. (1994) The role of magmatic and hydrothermal processes in the chemical evolution of the Strange Lake plutonic complex, Quebec-Labrador. *Contrib. Mineral. Petrol.* **118,** 33–47.

Brenan J. M., Shaw H. F., Ryerson F. J., and Phinney D. L. (1995) Experimental determination of trace-element partitioning between pargasite and a synthetic hydrous andesitic melt. *Earth Planet. Sci. Lett.* **135,** 1–11.

Brice J. C. (1975) Some thermodynamic aspects of the growth of strained crystals. *J. Cryst. Growth* **28,** 249–253.

Bryant C. J., Arculus R. J., and Chappell B. W. (1997) Clarence River supersuite: 250 Ma Cordilleran tonalitic I-type intrusions in eastern Australia. *J. Petrol.* **38,** 975–1001.

Cerny P. and Siilova J. (1980) The Tanco pegmatite at Bernic Lake, Manitoba, XII: Hafnian zircon. *Can. Mineral.* **18,** 313–321.

Charoy B. and Noronha B. F. (1996) Multistage growth of a rare-element, volatile-rich microgranite at Argemela (Portugal). *J. Petrol.* **37,** 73–94.

Cherniak D. J., Hanchar J. M., and Watson E. B. (1997) Diffusion of tetravalent cations in zircon. *Contrib. Mineral. Petrol.* **127,** 383–390.

David K., Schiano P., and Allegre C. J. (2000) Assessment of the Zr/Hf fractionation in oceanic basalts and continental materials during petrogenetic processes. *Earth Planet. Sci. Lett.* **178,** 285–301.

Della Ventura G., Bellatreccia F., and Williams C. T. (1999) Zr- and LREE-rich titanite from Tre Croci, Vico complex (Latium, Italy). *Mineral. Mag.* **63,** 123–130.

Dostal J. and Chatterjee A. K. (1995) Origin of topaz-bearing and related peraluminous granites of the Late Devonian Davis Lake pluton, Nova Scotia, Canada: Crystal versus fluid fractionation. *Chem. Geol.* **123,** 67–88.

Dupuy C., Liotard J. M., and Dostal J. (1992) Zr/Hf fractionation in intraplate basaltic rocks: Carbonate metasomatism in the mantle source. *Geochim. Cosmochim. Acta* **56,** 2417–2423.

Förster H.-J., Tischendorf G., Trumbull R. B., and Gottesmann B. (1999) Late-Collisional Granites in the Variscan Erzgebirge, Germany. *J. Petrol.* **40,** 1613–1645.

Fujinawa A. and Green T. H. (1997) Partitioning behaviour of Hf and Zr between amphibole, clinopyroxene, garnet and silicate melts at high pressure. *Eur. J. Mineral.* **9,** 379–391.

Green T. H. (1994) Experimental studies of trace-element partitioning applicable to igneous petrogenesis –Sedona 16 years later. *Chem. Geol.* **117,** 1–36.

Green T. H., Blundy J. D., Adam J., and Yaxley G. M. (2000) SIMS determination of trace element partition coefficients between garnet, clinopyroxene and hydrous basaltic liquids at 2–7.5 GPa and 1080–1200°C. *Lithos* **53,** 165–187.

Greenwood N. N. and Earnshaw A. (1984) *Chemistry of the Elements*. Pergamon Press, Oxford.

Harrison T. M. and Watson E. B. (1983) Kinetics of zircon dissolution and zirconium diffusion in granitic melts of variable water content. *Contrib. Mineral. Petrol.* **84,** 66–72.

Hart S. R. and Dunn T. (1993) Experimental cpx/melt partitioning of 24 trace elements. *Contrib. Mineral. Petrol.* **113,** 1–8.

Hauri E. H. and Hart S. R. (1997) Rhenium abundances and systematics in oceanic basalts. *Chem. Geol.* **139,** 185–205.

Hess P. C. (1991) The role of high field strength cations in silicate melts. *Chemistry of Magmas, Advances in Physical Geochemistry*, Vol. 9. (eds. L. L. Perchuk and I. Kushiro). Springer-Verlag, New York, pp. 152–191.

Jochum K. P Seufert H. M., Spettel B., and Palme H. (1986) The solar-system abundances of Nb, Ta, and Y, and the relative abundances of refractory lithophile elements in differentiated bodies. *Geochim. Cosmochim. Acta* **50,** 1173–1183.

Keppler H. (1993) Influence of fluorine on the enrichment of high field strength trace elements in granitic rocks. *Contrib. Mineral. Petrol.* **114,** 479–488.

Klein M., Stosch H. G., and Seck H. A. (1997) Partitioning of high field-strength and rare-earth elements between amphibole and quartz-dioritic to tonalitic melts: An experimental study. *Chem. Geol.* **138,** 257–271.

Kortemeirer W. T. and Burt D. M. (1988) Ongonite and topazite dikes in the Flying W ranch area, Tonto basin, Arizona. *Am. Mineral.* **73,** 507–523.

Kyle P. R., Moore J. A., and Thirwall M. F. (1992) Petrologic evolution of anorthoclase phonolite lavas at Mount Erebus, Ross Island, Antarctica. *J. Petrol.* **33,** 849–875.

Linnen R. L. and Keppler H. (1997) Columbite solubility in granitic melts: Consequences for the enrichment and fractionation of Nb and Ta in the Earth's crust. *Contrib. Mineral. Petrol.* **128,** 213–227.

Pan Y. (1997) Controls on the fractionation of isovalent trace elements in magmatic and aqueous systems: Evidence from Y/Ho, Zr/Hf, and lanthanide tetrad effect—A discussion of the article by M. Bau (1996). *Contrib. Mineral. Petrol.* **128,** 405–408.

Panter K. S., Kyle P. R., and Smellie J. L. (1997) Petrogenesis of a phonolite-trachyte succession at Mount Sidley, Marie Byrd Land, Antarctica. *J. Petrol.* **38,** 1225–1253.

Pichavant M., Herrera J. V., Boulmier S., Briqueu L., Joron J. L., Juteau M., Marin L., Michard A., Sheppard S. M. F., Treuil M., and Vernet M. (1988) The Macusani glasses, SE Peru: Evidence of chemical fractionation in peraluminous magmas. *Magmatic Processes: Physiochemical Principles*. (ed. B. O. Mysen), pp. 359–373 Special Publication, Vol. 1. Geochemistry Society.

Raimbault L., Cuney M., Azencott C., Duthou J. L., and Joron J. L. (1995) Geochemical evidence for a multistage magmatic genesis of Ta-Sn-Li mineralization in the granite at Beauvoir, French Massif Central. *Econ. Geol.* **90,** 548–576.

Shannon R. D. (1976) Revised effective ionic radii and systematic studies of interatomic distances in halides and chalcogenides. *Acta Cryst.* **A32,** 751–767.

Speer J. A. and Cooper B. J. (1982) Crystal structure of synthetic hafnon, $HfSiO_4$, comparison with zircon and the actinide orthosilicates. *Am. Mineral.* **67,** 804–808.

Taylor W. R., Esslemont G., and Sun S. -S. (1995) Geology of the volcanic-hosted Brockman rare-metals deposit, Halls Creek Mobile Zone, northwest Australia. II. Geochemistry and petrogenesis of the Brockman volcanics. *Mineral. Petrol.* **52,** 231–255.

van Westrenen W., Blundy J., and Wood B. (1999) Crystal-chemical controls on trace element partitioning between garnet and anhydrous silicate melt. *Am. Mineral.* **84,** 838–847.

van Westrenen W., Blundy J. D., and Wood B. J. (2000) Effect of Fe^{2+} on garnet-melt trace element partitioning: Experiments in FCMAS and quantification of crystal-chemical controls in natural systems. *Lithos* **53,** 189–201.

Wang R. C., Fontan F., Xu S. J., Chen X. M., and Monchoux P. (1996) Hafnian zircon from the apical part of the Suzhou granite, China. *Can. Mineral.* **34,** 1001–1010.

Watson E. B. (1979) Zircon saturation in felsic liquids: Experimental results and applications to trace element geochemistry. *Contrib. Mineral. Petrol.* **70,** 407–419.

Watson E. B. and Harrison T. M. (1983) Zircon saturation revisited: Temperature and composition effects in a variety of crustal magma types. *Earth Planet. Sci. Lett.* **64,** 295–304.

Wörner G., Beusen J. M., Duchateau N., Gijbels R., and Schmincke H. U. (1983) Trace element abundances and mineral/melt distribution coefficients in phonolites from the Laacher See volcano (Germany). *Contrib. Mineral. Petrol.* **84,** 152–173.